Sterile Neutrino Search at the NEOS Experiment

Y. J. Ko,[1] B. R. Kim,[2] J. Y. Kim,[3] B. Y. Han,[4] C. H. Jang,[1] E. J. Jeon,[5] K. K. Joo,[2] H. J. Kim,[6] H. S. Kim,[3] Y. D. Kim,[5,3,7] Jaison Lee,[5,*] J. Y. Lee,[6] M. H. Lee,[5] Y. M. Oh,[5,†] H. K. Park,[5,7] H. S. Park,[8] K. S. Park,[5] K. M. Seo,[3] Kim Siyeon,[1] and G. M. Sun[4]

(NEOS Collaboration)

[1]*Department of Physics, Chung-Ang University, Seoul 06974, Korea*
[2]*Department of Physics, Chonnam National University, Gwangju 61186, Korea*
[3]*Department of Physics and Astronomy, Sejong University, Seoul 05006, Korea*
[4]*Neutron Science Division, Korea Atomic Energy Research Institute, Daejeon 34057, Korea*
[5]*Center for Underground Physics, Institute for Basic Science (IBS), Daejeon 34047, Korea*
[6]*Department of Physics, Kyungpook National University, Daegu 41566, Korea*
[7]*University of Science and Technology, Daejeon 34113, Korea*
[8]*Korea Research Institute of Standards and Science, Daejeon 34113, Korea*

(Received 17 October 2016; published 21 March 2017)

An experiment to search for light sterile neutrinos is conducted at a reactor with a thermal power of 2.8 GW located at the Hanbit nuclear power complex. The search is done with a detector consisting of a ton of Gd-loaded liquid scintillator in a tendon gallery approximately 24 m from the reactor core. The measured antineutrino event rate is 1976 per day with a signal to background ratio of about 22. The shape of the antineutrino energy spectrum obtained from the eight-month data-taking period is compared with a hypothesis of oscillations due to active-sterile antineutrino mixing. No strong evidence of $3+1$ neutrino oscillation is found. An excess around the 5 MeV prompt energy range is observed as seen in existing longer-baseline experiments. The mixing parameter $\sin^2 2\theta_{14}$ is limited up to less than 0.1 for Δm^2_{41} ranging from 0.2 to 2.3 eV^2 with a 90% confidence level.

DOI: 10.1103/PhysRevLett.118.121802

The mixing among three neutrinos has been well established by experiments performed in the last two decades since the discovery of neutrino oscillations [1–3]. Consistent measurements of the two mass differences and the three mixing angles of the standard, three-neutrino mixing model have been reported by oscillation experiments using atmospheric, solar, reactor, and accelerator neutrinos [4]. Nevertheless, the mass hierarchy, the mass of the lightest neutrino, the Dirac or Majorana nature of the neutrino, and the CP phase are yet to be determined [5].

Even though the number of active light neutrinos is limited to three by Z boson decay-width measurements [6], it is still possible to have additional neutrinos if they are sterile. Sterile neutrinos can be identified by the occurrence of active-sterile neutrino oscillations. A hint for this is the LSND experiment's report of an observation of $\bar{\nu}_\mu \to \bar{\nu}_e$ mixing with a frequency corresponding to a mass-squared difference larger than 0.01 eV^2 [7]. Results from the MiniBooNE's test of the LSND signal are, however, inconclusive [8].

In addition to the LSND result, there are two other anomalies that could possibly be signs of active-sterile neutrino oscillations. An apparent ν_e disappearance over a baseline of a few meters in the GALLEX and SAGE gallium experiments exposed to radioactive sources was reported [9]; the ratio of the numbers of measured and predicted events is 0.88 ± 0.05. A number of short-baseline reactor antineutrino experiments established limits on the presence of neutrino oscillations with eV mass differences by shape analyses of the measured neutrino energy spectra. Among those experiments, the Bugey experimental limits on sterile neutrinos are the most stringent [10]. Mueller *et al.* [11] found about a 6% deficit in reactor antineutrino event rates compared with the theoretical expectations for the short-baseline reactor experiments, which is the so-called "reactor antineutrino anomaly" (RAA). It can be interpreted as an active-sterile neutrino oscillation with three active neutrinos plus one or more sterile neutrinos, i.e., a $3+n\nu$ scenario [12,13], compatible with the LSND result. Recent reactor experiments that measured the θ_{13} mixing angle, Daya Bay [14], RENO [15], and Double Chooz [16], all confirmed a similar deficit in the measured neutrino event rates. It is also intriguing that these three experiments observed a significant event excess beyond expectations from existing reactor-flux models [13,17,18] at prompt energies around 5 MeV.

The Planck satellite experiment [19] constrained the effective neutrino number to less than 3.7 at a 95% confidence level and excluded the existence of sterile neutrinos with masses near 1 eV fully thermalized in the early

Universe. However, theoretical models such as a large lepton asymmetry [20] or neutrino self-interactions [21] show that the effective number of sterile neutrinos can be much less than one. Therefore, light sterile neutrinos remain compatible with current cosmological constraints and should be searched for in more refined experiments with higher sensitivities. The phenomenology of light sterile neutrinos was recently reviewed in Ref. [22].

A search for sterile neutrinos at a nuclear reactor was first proposed by Mikaelyan [23]. Following the $3+1$ ν mixing scenario [24], the survival probability of a neutrino with energy E_ν at a distance L shorter than 100 m can be approximated as

$$P \simeq 1 - \sin^2 2\theta_{14} \sin^2 \left[1.27 \frac{\Delta m^2_{41} L}{E_\nu} \left(\frac{\mathrm{eV}^2 \cdot \mathrm{m}}{\mathrm{MeV}} \right) \right]. \quad (1)$$

A new oscillation parameter set of $(\sin^2 2\theta_{14},\ \Delta m^2_{41})$ introduced by the existence of an eV-scale light sterile neutrino can be obtained by measuring the distortion in the energy spectrum and/or a deficit from the expected number of inverse beta decay (IBD, $\bar{\nu}_e + p \rightarrow e^+ + n$) events at a short distance from a nuclear reactor core. Considering the IBD energy spectrum, which is smoothly peaked at around 3 MeV, the sensitivity for observing an ~ 1 eV^2 mass-squared difference becomes the highest at several meters and falls off as the distance increases. The Daya Bay experiment sets limits on a light sterile neutrino with lower (i.e., < 1 eV^2) mass-squared differences [25]. Currently, a number of short-baseline reactor experiments are being developed [26]. Here we report results from the NEOS (neutrino experiment for oscillation at short baseline) experiment for a light sterile neutrino search at a distance of 24 m from a reactor core.

The NEOS detector was installed in the tendon gallery of reactor unit 5 of the Hanbit Nuclear Power Complex in Yeonggwang, Korea. This is the same reactor complex being used for the RENO experiment [15]. The active core size of unit 5 is 3.1 m in diameter and 3.8 m in height and contains 177 low-enriched uranium fuel assemblies; about one-third of these assemblies are replaced with fresh ones every 18 months. The tendon gallery is located 10 m below ground level and is directly under the wall of the containment building. The minimum overburden with the ground and building structures corresponds to 20 m water equivalent. The detector is centered at 23.7 ± 0.3 m from the center of the reactor core, while the distance to the closest neighboring reactor core is 256 m.

The NEOS detector consists of a neutrino target, mineral oil buffers, passive shieldings, muon counters, and supporting structures (see Fig. 1). The positron annihilation followed by a neutron capture from an electron antineutrino IBD process is detected in the target, which is a horizontal cylindrical stainless-steel tank with a 1008 L inner volume (103 cm in diameter and 121 cm in length) filled with a

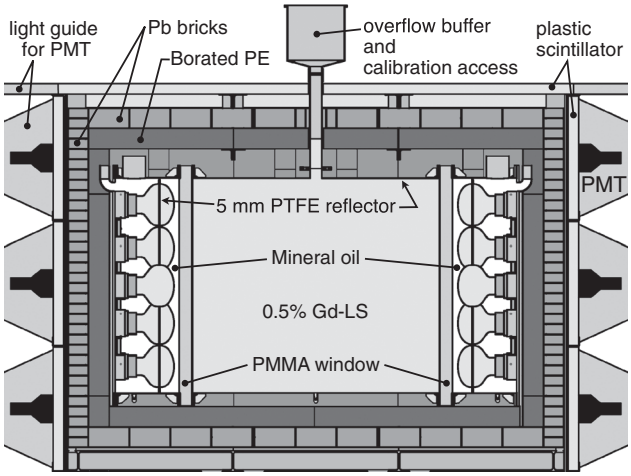

FIG. 1. A simplified cross-sectional view of the NEOS detector.

0.5% Gd-doped liquid scintillator [27]. Each end of the target vessel is viewed by 19 eight-inch photomultiplier tubes (PMTs) that are closely packed in mineral oil buffers. Each buffer and target are separated by a 6-cm-thick transparent polymethyl methacrylate (PMMA) window. Plates of 5-mm-thick polytetrafluoroethylene (PTFE) reflector are installed on the inner wall of the target vessel and along the PMT glasses' equator surfaces. The target tank is enclosed by a 10-cm-thick borated polyethylene (PE) and lead layers for shielding neutrons and external gamma rays, respectively. Muon counters made from 5-cm-thick plastic scintillators surround the outside of the detector.

The waveforms of all 38 PMTs are digitized and recorded by 500 megasampling (MS) per second flash analog-to-digital converter (ADC) modules, each of which makes an independent trigger decision. Signals from the muon counters are processed by a 62.5 MS/s ADC module. A trigger control board decides the global trigger and synchronizes the ADC modules. A trigger requiring 30 or more PMT signals higher than the 6 mV threshold is fully efficient for energies above 400 keV. The trigger rate was about 210 Hz. The detector operated for 46 days with the reactor off (t_{off}) and 180 days with the reactor on (t_{on}).

The detector was calibrated once every week with ^{137}Cs, ^{60}Co, ^{252}Cf, and PoBe sources. Continuous background events from several well-known radioactivities are used for additional calibrations. The charge to energy ratios of single gamma ray events show a nonlinear detector response as shown in Fig. 2(a). An empirical function used to describe this nonlinearity is

$$Q/E_\gamma = (p_0 + p_1 E_\gamma)[1 + p_2 \exp(p_3 \sqrt{E_\gamma})], \quad (2)$$

where Q is the charge, E_γ is the true γ energy, and p_i terms are fitting parameters. The detector stability and the nonuniform response along the horizontal axis of the detector are continuously monitored and corrected using

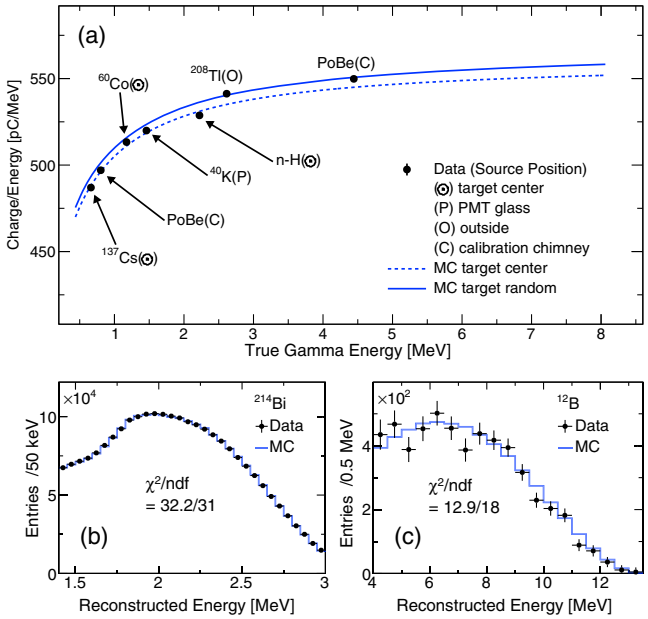

FIG. 2. Detector responses to γ and β sources: (a) ratios of full peak charges to the true γ energies, (b) β-decay spectra for ^{214}Bi, and (c) ^{12}B.

2.6 MeV external γ rays from ^{208}Tl and internal α background events.

The detector is simulated with a GEANT4-based Monte Carlo (MC) simulation [28]. The optical properties of the liquid scintillator and reflecting materials and responses of PMTs and electronics are fine-tuned to describe the source calibration data, and, consequently, the effects of escaping γ rays, energy resolution ($\sigma/E_\gamma \sim 5\%$ for a full peak at 1 MeV), and the nonlinear Q to E_γ response are well reproduced. The reconstructed energy spectra for ^{214}Bi and ^{12}B β decays are shown in Figs. 2(b) and 2(c) with the MC results superimposed. The systematic error on the energy scale associated with differences between the data and MC calculations is 0.5%.

The selection criteria of IBD candidate events are determined to maximize the signal to background ratio. We start with a pair of events which consists of a prompt event candidate that has an energy above 1 MeV and its following delayed event candidate of an n-Gd capture signal with an energy between 4 and 10 MeV in a 1–30 μs time window. To exclude multiple neutron-induced backgrounds, the pair is rejected when any events occur at a time that is less than 30 μs before or 150 μs after the prompt signal time. Pairs of which the prompt or delayed events occur in a 150 μs interval after a muon-counter hit are vetoed. Finally, pairs caused by the scattering and subsequent capture of fast neutrons are identified using a pulse shape discrimination (PSD) requirement that is adjusted to accept more than 99.9% of the electron-induced recoil events over the full energy range. The background fraction that is removed by the PSD requirement was measured to be 73% during the reactor-off period.

With these requirements, 1976.7 ± 3.4 (85.1 ± 1.4) IBD candidates per day were selected during the reactor-on (-off) period with the prompt energy between 1 and 10 MeV. No evidence was found for additional backgrounds associated with the reactor operation or for a significant background fluctuation in the whole running period. The muon-counter rate, to which the fast-neutron background is related, was stable at 241 Hz with a 2 Hz day-to-day rms variation. The energy distributions of the fast-neutron scattering events that were rejected by the PSD requirement show only small variations consistent with statistical fluctuations throughout the entire running period. Contributions from accidental background events were estimated by the time-delayed coincidences method [29] to be 7 ± 1 per day, where the error corresponds to the range of the daily variations.

The measured prompt energy spectrum (S_{neos}) is shown in Fig. 3(a), superimposed with the predicted nonoscillation spectra: one based on flux calculations by Huber [13] and Mueller (HM) [11] weighted by the IBD cross sections estimated by Vogel and Beacom [30] and another based on the Daya Bay reactor antineutrino spectrum [31]. The former and the latter predicted spectra are denoted as S_{hmv} and S_{dyb}, respectively, and their superscript 3ν (4ν) denotes the 3 (3 + 1) ν hypothesis. The predicted spectra are generated using the detector response shown in the inset in Fig. 3(a) produced by a full simulation of IBD events of which the $\bar{\nu}_e + p$ reaction occurs at random positions throughout the detector target and produced e^+ and n are propagated through all of the detector responses. The antineutrinos are assumed to originate uniformly throughout the cylindrical active reactor core, and the average primary element fission fractions of 0.655, 0.072, 0.235, and 0.038 for ^{235}U, ^{238}U, ^{239}Pu, and ^{241}Pu, respectively, are used. The differences between the fission fractions for the NEOS data and the ones for Daya Bay are taken into account, and small corrections are made using the HM flux model as instructed in Ref. [31].

The excess around 5 MeV versus $S^{3\nu}_{\text{hmv}}$ is clearly seen, as shown in Figs. 3(a) and 3(b), for the first time at this short baseline, whereas previous short-baseline measurements [10,32] did not show a clear excess. The excess does not completely disappear even when the data are divided by $S^{3\nu}_{\text{dyb}}$, as shown in Fig. 3(c). This can be explained as that the excess can be contributed differently from each fission element [33]. It is, however, difficult to conclude with the current level of uncertainties. Another large discrepancy other than the 5 MeV excess for the $S^{3\nu}_{\text{hmv}}$ case is found at the lowest energy range. The disagreement is as large as 8% at 1 MeV and drops rapidly as the energy increases. For the incident antineutrino flux below 2 MeV and above 8 MeV, where tabulated data do not exist, we used the exponential functions in Refs. [11,33] for an extrapolation. For the

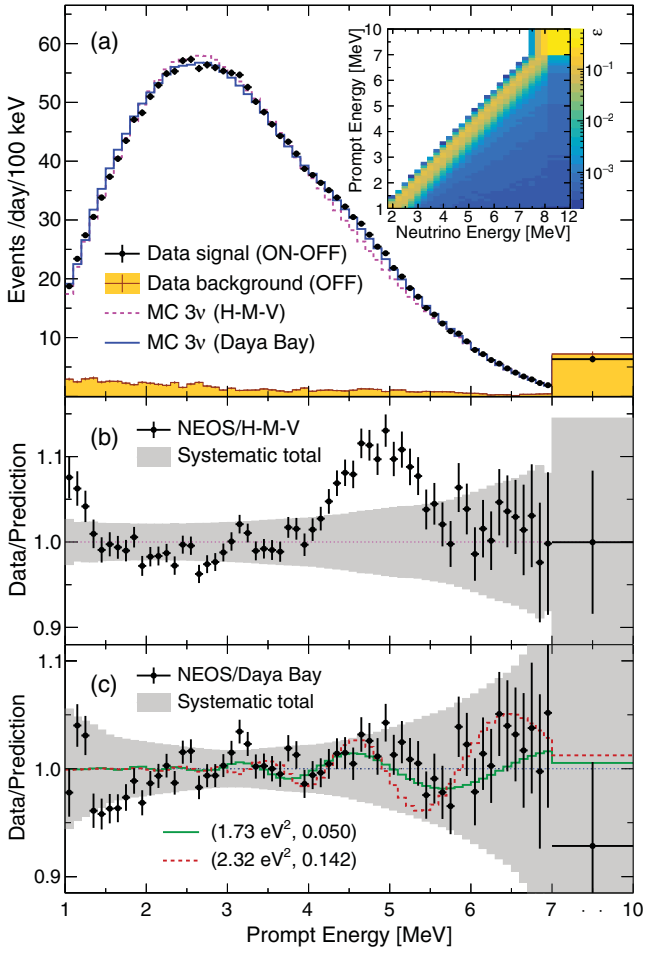

FIG. 3. (a) The IBD prompt energy spectrum. The last bin is integrated up to 10 MeV. The orange shaded histogram is the background spectrum measured during the reactor-off period. The detector response matrix in the inset shows the relation between the neutrino energy and the prompt energy. (b) The ratio of the observed prompt energy spectrum to the HM flux prediction weighted by the IBD cross section with the $3-\nu$ hypothesis. The predicted spectrum is scaled to match the area of the data excluding the 5 MeV excess region (3.4–6.3 MeV). (c) The ratio of the data to the expected spectrum based on the Daya Bay result with the 3ν hypothesis, scaled to match the whole data area. The solid green line is the expected oscillation patterns for the best fit of the data to the $3+1$ ν hypothesis and the corresponding oscillation parameters $(\sin^2 2\theta_{14}, \Delta m^2_{41})$ is $(0.05, 1.73\ \mathrm{eV}^2)$. The dashed red line is the expected oscillation pattern for the RAA best fit parameters $(0.142, 2.32\ \mathrm{eV}^2)$. The gray error bands in (b) and (c) are estimated total systematic uncertainties, corresponding to the square roots of diagonal elements of the covariance matrices.

comparison with S_{dyb}, the fluctuation shown in the lowest energy range is mainly due to the convolution of the spectrum from the original one with large neutrino energy bin sizes to one with finer prompt energy bin sizes for this work. Other small fluctuations at several energies also seem to have some small structures which are common for both reference spectra but, regarding the uncertainties, are not so significant.

The following systematic uncertainties are taken into account. Errors in the reference antineutrino spectra are the main contributors to the total uncertainties. The 0.5% uncertainty in the reconstructed energy scale is another large contributor to the total uncertainty. Other sources of uncertainty, such as the inaccuracy of the effective baseline, fuel-related uncertainties from burn-up and fission fractions, spill-in from inactive volumes, events generated by antineutrinos from neighbor reactors, and other detector-related uncertainties have negligible effects on the spectral shape.

Probing an oscillation in a spectrum measured with a single detector at one fixed distance from the reactor core depends on the accuracy and precision of the reference spectrum. Among the available references, the flux calculation by Huber and Mueller provides tabulated uncertainties with their correlations between the neutrino energy bins and isotopes, and, even though their uncertainties are underestimated [18], their spectral shapes (not their absolute rates) are generally in good agreement with existing experimental results except for the region of the 5 MeV excess. A recent high-resolution *ab initio* calculation by Dwyer and Langford [17] better describes the observed 5 MeV excess, but its large uncertainties and their correlations, which are yet to be exactly quantified, make a comparison with our data impractical. Experimentally, only the Daya Bay unfolded spectrum [31] is based on a direct measurement, and, therefore, the uncertainties in the antineutrino spectrum are relatively small. The correlation of uncertainties among the energy bins can be dealt with by the provided covariance matrix.

In the present work, the measured prompt energy spectrum is compared with S_{dyb} for testing the oscillation. A χ^2 is constructed with 61 data points in the 1–10 MeV prompt energy spectrum and a covariance matrix V_{ij} that accounts for correlations between uncertainties:

$$\chi^2 = \sum_{i=1}^{N}\sum_{j=1}^{N}\left(M_i - \frac{t_{\mathrm{on}}}{t_{\mathrm{off}}}B_i - T_i\right)V_{ij}^{-1} \times \left(M_j - \frac{t_{\mathrm{on}}}{t_{\mathrm{off}}}B_j - T_j\right), \quad (3)$$

where M (B) is the number of measured IBD candidate events accumulated during the reactor-on (-off) period, T is the prediction from a reference spectrum that accounts for oscillation parameters, and the subscripts i and j denote the prompt energy bin. To construct V_{ij}, the elements for the errors in the reference antineutrino spectrum are calculated from the matrix in Table 13 of Ref. [31], by convolving them with the detector response shown in the inset in Fig. 3(a). Then the other elements from statistical and detector systematic uncertainties are added.

The χ^2 values are calculated on a fine grid in the sensitive Δm^2_{41} range from 0.06 to 6 eV^2. The χ^2 value with the 3ν hypothesis is $\chi^2_{3\nu}/\mathrm{NDF} = 64.0/61$, where NDF denotes the number of degrees of freedom. The minimum χ^2 value with the $3+1$ ν hypothesis, $\chi^2_{4\nu}/\mathrm{NDF} = 57.5/59$, is obtained at $(\sin^2 2\theta_{14}, \Delta m^2_{41}) = (0.05, 1.73\ \mathrm{eV}^2)$, and the second minimum at $(0.04, 1.30\ \mathrm{eV}^2)$ has a similar χ^2 value to the first one. The values of the mass-squared differences of the two minima are compatible with the latest global fit results [22,34], though the mixing angle parameters, $\sin^2 2\theta_{14}$, are smaller than those global best fit values. The p value corresponding to the χ^2 difference between the 3ν hypothesis and the best fit for the $3+1$ ν hypothesis, $\Delta\chi^2 = \chi^2_{3\nu} - \chi^2_{4\nu} = 6.5$, is estimated to be 22% using a large number of Monte Carlo data sets with statistical and systematic fluctuations [35]. As a result, no apparent parameter set of $(\sin^2 2\theta_{14}, \Delta m^2_{41})$ that has significant favor for the $3+1$ ν hypothesis is found.

The limit on the $\sin^2 2\theta_{14}$ value for each Δm^2_{41} is found using a raster scan [36]. For a Δm^2_{41} value, a probability density function $f(\sin^2 2\theta_{14})$ is constructed from the $\Delta\chi^2$ distribution in the $\sin^2 2\theta_{14}$ range from 0 to 1, where $\Delta\chi^2$ is the difference between a χ^2 value at a $\sin^2 2\theta_{14}$ point and the minimum χ^2 value at the corresponding Δm^2_{41}. The upper limit (ul) at confidence level (C.L.) of $1-\alpha$ is found with the condition of

$$\int_{ul}^{1} f(\sin^2 2\theta) d(\sin^2 2\theta) = \alpha. \quad (4)$$

The resulting exclusion limits at 90% C.L. are shown in Fig. 4, superimposed with the 90% C.L. exclusion curves of the Bugey-3 [10] and the Daya Bay [37] limits and with the allowed region by the RAA fit from Fig. 8 in Ref. [12]. The mixing angle parameter $\sin^2 2\theta_{14}$ is excluded for the region significantly less than 0.1 for the $0.2\ \mathrm{eV}^2 < \Delta m^2_{41} < 2.3\ \mathrm{eV}^2$ range. Our limits are compatible with the Bugey-3 result at the $0.2\ \mathrm{eV}^2 < \Delta m^2_{41} < 4\ \mathrm{eV}^2$ range, since the baselines of the two experiments are similar. The Bugey-3 and the Daya Bay are more sensitive than the NEOS at lower Δm^2_{41} because of their spans of longer baselines. At above 4 eV^2, our sensitivity drops as a natural consequence of the shape-only analysis, while the Bugey-3 and the Daya Bay limits converge to constant $\sin^2 2\theta_{14}$ values, since the absolute rates are taken into account based on the ILL-Vogel [38,39] and Huber-Mueller flux models in their analyses, respectively. Our limit curve shows a more ragged shape than that of Bugey-3, because the differences between the data and the model spectrum are more significant by higher statistics and by use of the Daya Bay model spectrum which has smaller errors around the spectral peak range. For a more practical comparison and/or combined analysis of this work with the Bugey-3 data, it would be necessary to revise the Bugey-3 data with the Daya Bay absolute spectrum, which should be more realistic for measurements using similar types of commercial reactors.

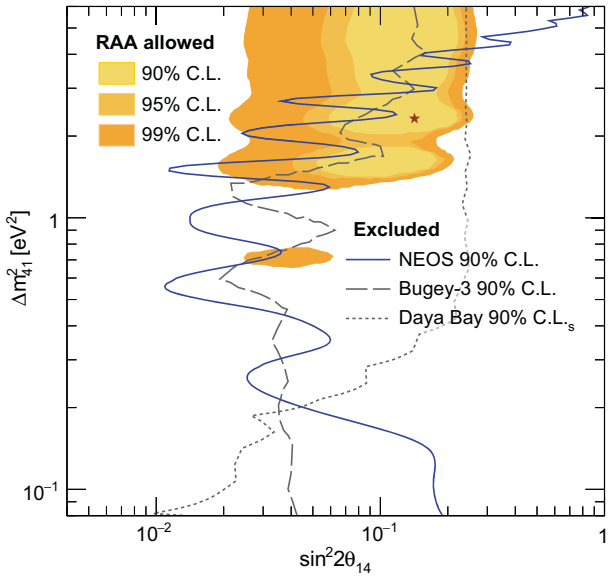

FIG. 4. Exclusion curves for $3+1$ neutrino oscillations in the $\sin^2 2\theta_{14} - \Delta m^2_{41}$ parameter space. The solid blue curve is 90% C.L. exclusion contours based on the comparison with the Daya Bay spectrum, and the dashed gray curve is the Bugey-3 90% C.L. result [10]. The dotted curve shows the Daya Bay 90% C.L.$_s$ result [37]. The shaded area is the allowed region from the reactor antineutrino anomaly fit, and the star is its optimum point [12].

In conclusion, no strong evidence for $3+1$ neutrino oscillations is observed in this study. We could set up new stringent upper limits on the θ_{14} mixing angle for the $\Delta m^2_{41} \sim 1\ \mathrm{eV}^2$ region, thanks to the high signal to background ratio, good energy resolution, and using the most realistic reference antineutrino spectrum. The results are currently limited by uncertainties in the reference spectrum of the Daya Bay and systematics of the NEOS data. The systematic uncertainties in the antineutrino spectrum will be reduced if the reference spectrum from the RENO experiment is available, since it uses the same reactor complex. Other ongoing or scheduled experiments [40–43] with even shorter baselines and/or better L/E resolution are expected to improve the sensitivities. It should be remarked that, in addition to these short-baseline sterile neutrino searches, future long-baseline reactor antineutrino experiments [44,45] aimed at the determination of the neutrino mass hierarchy would require more accurate reference IBD spectra. Recently, the IceCube and MINOS experiments constrained the θ_{24} mixing angle for the $3+1$ ν model and rejected the LSND anomaly parameter space for $\Delta m^2_{41} < 3\ \mathrm{eV}^2$ [46,47], for which the former assumed θ_{14} values from the global fits [34,48] and the latter combined θ_{14} constraints from the Daya Bay and the Bugey-3 results [37]. Our new limit will further improve the constraints to

the LSND anomaly parameter space by combining with the θ_{24} measurements.

This work is supported by IBS-R016-D1 and 2012M2B2A6029111 from National Research Foundation (NRF). We appreciate the Korea Hydro and Nuclear Power (KHNP) company and especially acknowledge the help and support provided by staff members of the Safety and Engineering Support Team of Hanbit Nuclear Power Plant 3. We appreciate the Daya Bay Collaboration for the discussion on the errors in their reference spectrum.

*jsahnlee@ibs.re.kr
†yoomin@ibs.re.kr

[1] Y. Fukuda *et al.* (Super-Kamiokande Collaboration), Phys. Rev. Lett. **81**, 1562 (1998).
[2] Q. R. Ahmad *et al.* (SNO Collaboration), Phys. Rev. Lett. **89**, 011301 (2002).
[3] K. Eguchi *et al.* (KamLAND Collaboration), Phys. Rev. Lett. **90**, 021802 (2003).
[4] G. L. Fogli, E. Lisi, A. Marrone, D. Montanino, A. Palazzo, and A. M. Rotunno, Phys. Rev. D **86**, 013012 (2012).
[5] C. Giunti and C. W. Kim, *Fundamentals of Neutrino Physics and Astrophysics* (Oxford University, New York, 2007).
[6] S. Schael *et al.* (SLD Electroweak Group, DELPHI, ALEPH, SLD, SLD Heavy Flavour Group, OPAL, LEP Electroweak Working Group, L3 Collaboration), Phys. Rep. **427**, 257 (2006).
[7] C. Athanassopoulos *et al.* (LSND Collaboration), Phys. Rev. Lett. **77**, 3082 (1996).
[8] A. A. Aguilar-Arevalo *et al.* (MiniBooNE Collaboration), Phys. Rev. Lett. **110**, 161801 (2013).
[9] J. N. Abdurashitov *et al.*, Phys. Rev. C **73**, 045805 (2006).
[10] B. Achkar *et al.*, Nucl. Phys. **B434**, 503 (1995).
[11] T. A. Mueller *et al.*, Phys. Rev. C **83**, 054615 (2011).
[12] G. Mention, M. Fechner, T. Lasserre, T. A. Mueller, D. Lhuillier, M. Cribier, and A. Letourneau, Phys. Rev. D **83**, 073006 (2011).
[13] P. Huber, Phys. Rev. C **84**, 024617 (2011); **85**, 029901(E) (2012).
[14] F. P. An *et al.* (Daya Bay Collaboration), Phys. Rev. Lett. **116**, 061801 (2016).
[15] J. H. Choi *et al.* (RENO Collaboration), Phys. Rev. Lett. **116**, 211801 (2016).
[16] Y. Abe *et al.* (Double Chooz Collaboration), Phys. Rev. Lett. **108**, 131801 (2012).
[17] D. A. Dwyer and T. J. Langford, Phys. Rev. Lett. **114**, 012502 (2015).
[18] A. C. Hayes, J. L. Friar, G. T. Garvey, G. Jungman, and G. Jonkmans, Phys. Rev. Lett. **112**, 202501 (2014).
[19] P. A. R. Ade *et al.* (Planck Collaboration), Astron. Astrophys. **594**, A13 (2016).
[20] J. Hamann, S. Hannestad, G. G. Raffelt, I. Tamborra, and Y. Y. Y. Wong, Phys. Rev. Lett. **105**, 181301 (2010).
[21] S. Hannestad, R. S. Hansen, and T. Tram, Phys. Rev. Lett. **112**, 031802 (2014).
[22] S. Gariazzo, C. Giunti, M. Laveder, Y. F. Li, and E. M. Zavanin, J. Phys. G **43**, 033001 (2016).
[23] L. Mikaelyan and V. Sinev, Yad. Fiz. **62**, 2177 (1999) [Phys. At. Nucl. **62**, 2008 (1999)].
[24] C. Giunti and M. Laveder, Phys. Rev. D **84**, 073008 (2011).
[25] F. P. An *et al.* (Daya Bay Collaboration), Phys. Rev. Lett. **117**, 151802 (2016).
[26] P. Vogel, L. Wen, and C. Zhang, Nat. Commun. **6**, 6935 (2015).
[27] B. R. Kim *et al.*, arXiv:1511.05551.
[28] S. Agostinelli *et al.* (GEANT4 Collaboration), Nucl. Instrum. Methods Phys. Res., Sect. A **506**, 250 (2003).
[29] Y. Abe *et al.* (Double Chooz Collaboration), Phys. Rev. D **86**, 052008 (2012).
[30] P. Vogel and J. F. Beacom, Phys. Rev. D **60**, 053003 (1999).
[31] F. P. An *et al.* (Daya Bay Collaboration), Chin. Phys. C **41**, 013002 (2017).
[32] H. Kwon, F. Boehm, A. A. Hahn, H. E. Henrikson, J. L. Vuilleumier, J. F. Cavaignac, D. H. Koang, B. Vignon, F. Von Feilitzsch, and R. L. Mossbauer, Phys. Rev. D **24**, 1097 (1981).
[33] P. Huber, Phys. Rev. Lett. **118**, 042502 (2017).
[34] J. Kopp, P. A. N. Machado, M. Maltoni, and T. Schwetz, J. High Energy Phys. 05 (2013) 050.
[35] See Supplemental Material at http://link.aps.org/supplemental/10.1103/PhysRevLett.118.121802 for more details.
[36] L. Lyons, arXiv:1404.7395.
[37] P. Adamson *et al.* (MINOS, Daya Bay Collaboration), Phys. Rev. Lett. **117**, 151801 (2016).
[38] K. Schreckenbach, G. Colvin, W. Gelletly, and F. Von Feilitzsch, Phys. Lett. B **160**, 325 (1985).
[39] P. Vogel, Phys. Rev. D **29**, 1918 (1984).
[40] N. Ryder (SoLid Collaboration), *Proc. Sci.*, EPS-HEP2015 (2015) 071.
[41] J. Ashenfelter *et al.* (PROSPECT Collaboration), arXiv:1309.7647.
[42] V. Hélaine, arXiv:1604.08877.
[43] I. Alekseev *et al.*, J. Instrum. **11**, P11011 (2016).
[44] F. An *et al.* (JUNO Collaboration), J. Phys. G **43**, 030401 (2016).
[45] S.-B. Kim, Nucl. Part. Phys. Proc. **265–266**, 93 (2015).
[46] M. G. Aartsen *et al.* (IceCube Collaboration), Phys. Rev. Lett. **117**, 071801 (2016).
[47] P. Adamson *et al.* (MINOS Collaboration), Phys. Rev. Lett. **117**, 151803 (2016).
[48] J. M. Conrad, C. M. Ignarra, G. Karagiorgi, M. H. Shaevitz, and J. Spitz, Adv. High Energy Phys. **2013**, 163897 (2013).